Annals of Biomedical Engineering, Vol. 38, No. 10, October 2010 *(© 2010)* pp. 3218–3225
DOI: 10.1007/s10439-010-0080-9

Respiratory Rate Extraction Via an Autoregressive Model Using the Optimal Parameter Search Criterion

J. Lee and K. H. Chon

Department of Biomedical Engineering, Worcester Polytechnic Institute, 100 Institute Road, Worcester, MA 01609, USA

(Received 2 December 2009; accepted 15 May 2010; published online 25 May 2010)

Associate Editor Leonidas D. Iasemidis oversaw the review of this article.

Abstract—We present an autoregressive model-based method which enables accurate respiratory rate extraction from pulse oximeter recordings over a wide range: 12–48 breaths/min. The method uses the optimal parameter search (OPS) technique to estimate accurate AR parameters which are then factorized into multiple pole terms. The pole with the highest magnitude is shown to correspond to the respiratory rate. The performance of the proposed method to extract respiratory rate is compared to the widely used Burg algorithm using both simulation examples and pulse oximeter recordings. In a previous study, we demonstrated several nonparametric time–frequency approaches that were more accurate than Burg's algorithm when the data length was 1 min [Chon, K. H., S. Dash, and K. Ju. *IEEE Trans. Biomed. Eng*. 56(8):2054–2063, 2009]. One of the key advantages of the AR method is that a shorter data length can be used. Thus, in this study, we reduced the data length to 30 s and applied our OPS algorithm to examine if accurate respiratory rates can be extracted directly from pulse oximeter recordings. It was found that our proposed method's accuracy was consistently better with smaller variance than Burg's method. In particular, our proposed method's accuracy was significantly greater when respiratory rates were lower than 24 breaths/min.

Keywords—Optimal parameter search, AR model, Respiratory rate, Pulse oximeter, Time–frequency spectrum.

INTRODUCTION

The pulse oximeter is widely used in clinical settings for measurement of heart rate and arterial oxygen saturation. Recently, much effort has centered on extracting additional vital sign information from a pulse oximeter; one such vital sign is extraction of the respiratory rate information. Various novel signal processing approaches have been used for the extraction, and promising results were obtained using nonparametric time–frequency spectral analysis[8] and a parametric time-invariant method based on an autoregressive (AR) model.[5] In a recent work, we have shown that our high resolution time–frequency analysis[11] of the pulse oximeter signal followed by taking the power spectrum of the extracted frequency modulation signal around the heart rate frequency resulted in the best accuracy among all compared methods, including the time-invariant AR method.[3] While the AR method was not as accurate as the time–frequency methods, it has many attractive features because it is more computationally efficient and works reasonably well even with short data records.[3,5] We conjecture that one of the key reasons it did not perform as well as other methods was due to an inefficient model order search criterion, namely, its reliance on the Akaike information criterion (AIC). Further, an arbitrary decision regarding the proper choice of the poles and the phase related to the estimated AR coefficients had to be made in order to extract the correct respiratory rate,[5] which can also compromise its accuracy.

We have previously developed one of the most efficient model order search criteria for AR-based methods, termed the optimal parameter search (OPS), which can be used for both time-invariant and time-varying signals.[6,14] Adopting the robust OPS method, the aforementioned limitations of the previously used AR method for extraction of respiratory rate can be mitigated. Thus, the goal of this work was to investigate the efficiency gained by using the OPS instead of the AIC for extraction of respiratory rates from pulse oximeter recordings of 23 human subjects. The other aim was to systematically investigate the effect of data length dependence on the accuracy of respiratory rate estimation. In particular, we were interested in the accuracy of these methods when the data length was as

Address correspondence to J. Lee, Department of Biomedical Engineering, Worcester Polytechnic Institute, 100 Institute Road, Worcester, MA 01609, USA. Electronic mail: jinseok@wpi.edu, gonasago@gmail.com

few as 30 s instead of the previous requirement of 60 s.[3] Finally, we examined if the proposed AR model technique provided better respiratory estimates when the respiratory frequency was higher than 36 breaths/min, as the previous methods' accuracy was limited to 36 breaths/min.[3,11] Our proposed OPS-based AR method was compared to the Burg's algorithm to systematically examine the pros and cons of the each method.

METHODS

Respiratory Rate Extraction with AR Model

Our approach to extracting respiratory rate from photoplethysmogram (PPG) waveforms is to use an AR model with a proven and efficient model order criterion known as the OPS.[6] Extraction of respiratory rates starts with an AR model:

$$x(n) = -\sum_{k=1}^{p} a_k x(n-k) + e(n), \tag{1}$$

where p is the model order, a_k are the unknown coefficients, and $e(n)$ is the prediction error. We use the OPS to obtain accurate parameter estimation among over-determined model order p. Details concerning the OPS are described in our previous publications.[6] Automatic selection of the candidate terms using the OPS is detailed in the proceeding section. The OPS has been thoroughly tested both by using simulation examples and by application to many diverse physiological signals.[4,12] In all cases, the OPS has been shown to be more accurate than the AIC, minimum description length (MDL) and the fast orthogonal search criterion.[4,10,12,13] Once the unknown AR parameters, a_k, are estimated, they are formulated as the transfer function $H(z)$ as shown below:

$$H(z) = \frac{1}{\sum_{k=1}^{p} a_k z^{-k}} = \frac{z^p}{(z-z_1)(z-z_2)\cdots(z-z_p)}, \tag{2}$$

where the AR coefficients are factorized into p pole terms. The real and complex conjugate poles define the power spectral peaks with higher magnitude poles corresponding to higher magnitude peaks. The resonant frequency of each spectral peak is given by the phase angle of the corresponding pole; thus, the phase angle θ of a pole at frequency f is defined as $2\pi f\Delta t$, where Δt is the sampling interval. If multiple poles are present (e.g. $p > 3$), the pole with the highest magnitude is chosen to be representative of the respiratory rate in the region of interest. In this paper, we set the frequency region of interest between 0.15 and 0.9 Hz for all PPG signals, and 0.15–0.7 Hz for simulation data. While the pole with the highest magnitude represents the heart rate for the PPG signal, we limit the region of interest to below 1 Hz since we are primarily interested in estimating the respiratory rate which should be the dominant pole within the above defined frequency region of interest.

The AR model respiratory rate extraction approach requires prefiltering of the PPG waveforms in order to minimize the cardiac effects. Thus, the PPG waveforms are detrended, filtered, and downsampled to 2 Hz so that we can increase the angular resolution between 0 and 1 Hz.

To illustrate the AR model-based respiratory rate extraction, a simple simulation example is provided with Burg's AR model algorithm, which is one of the widely used approaches in practice.[1,2,9] The test signal involves two frequencies chosen so that they represent the frequency responses of the heart rate and the normal respiratory rate as shown below:

$$y(n) = A_{\mathrm{h}} \cos\left(2\pi f_{\mathrm{h}}(n)\frac{n}{f_{\mathrm{s}}} + \phi_{\mathrm{h}}\right) + A_{\mathrm{b}} \cos\left(2\pi f_{\mathrm{b}}(n)\frac{n}{f_s} + \phi_{\mathrm{b}}\right), \tag{3}$$

where $f_{\mathrm{h}}(n)$ and $f_{\mathrm{b}}(n)$ are the heart rate and respiratory rate, respectively. ϕ_{h} and ϕ_{b} are phases associated with the heart rate and respiratory rate, respectively, and f_{s} is the sampling rate. We chose the model of Eq. (3) since the PPG waveform shown in Fig. 1 exhibits sinusoidal oscillatory characteristics. For the simulation example, A_{h} and A_{b} were set to 10 and 1, respectively. The parameters $f_{\mathrm{h}}(n)$ and $f_{\mathrm{b}}(n)$ were set to 1.0 and 0.3 Hz, respectively, and ϕ_{h} and ϕ_{b} were randomly generated between 0 and 2π with uniform distribution. We generated 6,000 samples with a sampling rate of 100 Hz which results in 1 min of data. To increase the angular resolution of the low frequency information, each windowed waveform was

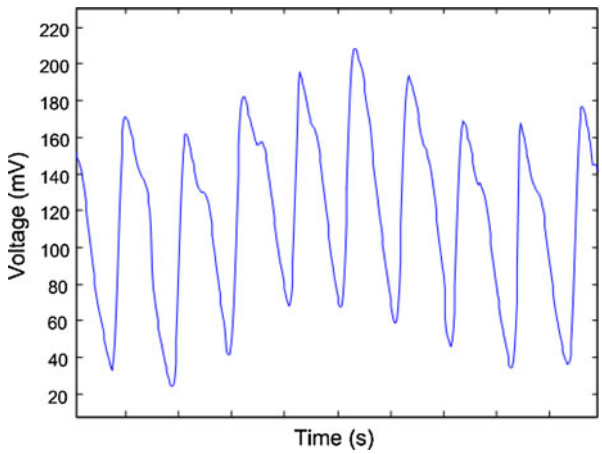

FIGURE 1. Representative pulse oximeter signal.

downsampled to 2 Hz. Based on the use of AIC, we selected an AR model order of 20, and the calculated AR parameters were transformed via the transfer function of Eq. (2). The resultant poles are shown in Fig. 2, and we list those poles with highest magnitudes in Table 1. Note that since the windowed waveform was downsampled to 2 Hz, the poles are limited to 1 Hz due to the Nyquist theorem. Among the poles, we set the region of interest for respiratory rates between 0.15 and 0.7 Hz, which is denoted as solid lines in Fig. 2. As shown in Table 1, the highest magnitude value among the poles listed is indicated in bold font; the corresponding angle results in the respiratory rate of 0.2983 Hz, which is close to the true respiratory rate of 0.3 Hz.

Model Selection with Optimal Parameter Search Algorithm

For the identification of a model order, the AIC and MDL are the two most widely used techniques. However, the limitations of the AIC and MDL criteria are well documented.[7] One of the main disadvantages of these methods is that because they provide only the maximum model order, subsequent least-squares estimation yields all parameters pertaining to the maximum model order, regardless of whether or not there are missing model terms. Thus, the resultant parameter estimate may become severely biased if there exist many missing terms within the maximum model order. The previous AR technique for estimating respiratory rates relied on the AIC for model order determination. Further compounding the problem is that the AR model order needs to be tuned to an individual, specific age groups or specific time periods. One way to avoid this problem is to have a sufficiently large sample size so that an average value could be obtained, but certainly this is difficult to accomplish.

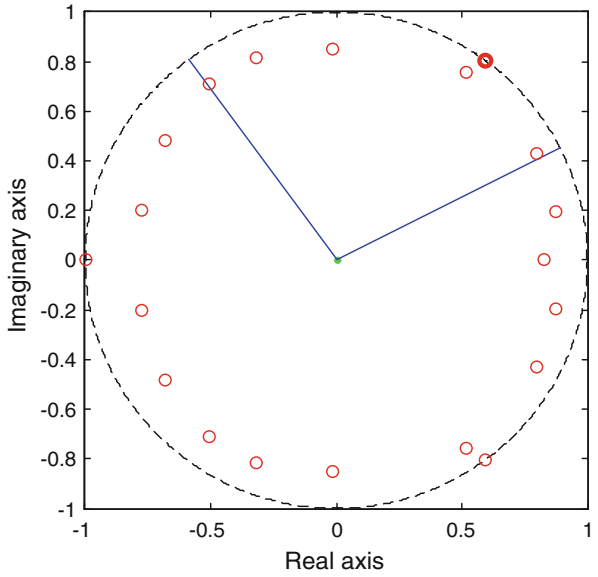

FIGURE 2. Poles of AR model with the model order of 20 are plotted, and the magnitudes of poles in the range of interest (0.15–0.7 Hz) are compared for respiratory rate extraction.

Our previously developed OPS algorithm overcomes the main limitations of the AIC and MDL. In addition, the OPS can be designed to automatically select the optimal model order for any signal, thus, can be tuned to each signal without any human subjectivity.

Details regarding the OPS have been previously documented,[6] thus will be only briefly summarized. With an initial model order selection of p_{ini}, the OPS algorithm is designed to select only the linearly independent vectors from the pool of candidate vectors. For Eq. (1) with the selected model order of p_{ini}, the candidate vectors are the following: $x(n-1)$, …, $x(n-p_{\text{ini}})$. These candidate vectors can be arranged as the matrix shown in Eq. (4), where N is the total number of data points.

$$\begin{matrix} x(0) & x(-1) & \cdots & x(1-p_{\text{ini}}) \\ x(1) & x(0) & \cdots & x(2-p_{\text{ini}}) \\ \vdots & \vdots & \cdots & \vdots \\ x(n-1) & x(n-2) & \cdots & x(n-p_{\text{ini}}) \\ \vdots & \vdots & \cdots & \vdots \\ x(N-1) & x(N-2) & \cdots & x(N-p_{\text{ini}}) \end{matrix} \tag{4}$$

The first step toward achieving linear independence among candidate vectors is to select $x(n-1)$ as the first candidate vector. The next candidate vector $x(n-2)$, and the first candidate vector $x(n-1)$, are then used to determine linear independence using $x(n-1)$ to fit $x(n-2)$ using the least-squares method and calculating the error between $x(n-2)$ and the estimated vector. Once it has been determined that $x(n-2)$ is a linear independent candidate vector, the vectors $x(n-1)$ and $x(n-2)$ are used to estimate the candidacy of the linear independence of $x(n-3)$. This procedure is continued until all the linearly independent vectors are selected to form a new candidate

TABLE 1. Candidate poles and corresponding angles and magnitudes.

Candidate poles	0.8002 + *j*0.4312	0.5916 + *j*0.8054	0.5169 + *j*0.7568	−0.0148 + *j*0.8520	−0.3181 + *j*0.8171	−0.5074 + *j*0.7078
Pole angle	0.1573	**0.2983**	0.3093	0.5055	0.6182	0.6980
Pole magnitude	0.9090	**0.9994**	0.9165	0.8522	0.8768	0.8709

vector pool. With the new candidate pool of R linearly independent vectors, least-squares analysis is performed on the following equation:

$$x(n) = \theta_{\mathrm{m}}^{\mathrm{T}}\phi + e(n), \tag{5}$$

where

$$\theta_{\mathrm{m}} = [g_0, g_1, \ldots, g_{\mathrm{R}}]^{\mathrm{T}}, \quad \text{and} \quad \phi = [w_0, w_1, \ldots, w_{\mathrm{R}}].$$

To minimize the error in Eq. (5), the cost function in Eq. (6) is used and parameter estimates can be according to Eq. (7)

$$J_{\mathrm{N}}(\theta_{\mathrm{m}}) = \left[x(n) - \theta_{\mathrm{m}}^{\mathrm{T}}\phi\right]^2. \tag{6}$$

$$\widehat{\theta_{\mathrm{m}}} = \left[\phi\phi^{\mathrm{T}}\right]^{-1}\phi x(n). \tag{7}$$

The projection distance is calculated as:

$$c_m = \frac{1}{N}\sum_{n=1}^{N}\widehat{\theta_m}^2 w_m(n)^2, \quad m = 1, \ldots R. \tag{8}$$

With an initial model order of p_{ini}, the significant model order p_{opt} is determined by the ratio of two neighboring projection distances[14] described as:

$$p_{\mathrm{opt}} = \arg\max_{m\in\{1,\cdots,p_{\mathrm{ini}}\}}\left(\frac{c_{m-1} - c_m}{c_m}\cdot 100 \geq \tau_{\mathrm{th}}\right), \tag{9}$$

where c_m is the mth longest projection distance and τ_{th} is a threshold percentage. We have shown that a τ_{th} value of 25 works well in most cases.[6,14]

Performance Comparison Under Color and White Noise Perturbation

To illustrate the advantage of the OPS-based respiratory rate extraction, we simulated the previous example but with both white and colored noise added, and the results were compared to Burg's algorithm. To examine the effect of colored noise, the simulated signal contained three frequencies representing the heart rate signal, denoted as $f_{\mathrm{h}}(n) = 1.0$ Hz, the respiratory rate signal, denoted as $f_{\mathrm{b}}(n) = 0.3$ Hz, and the noise signal, denoted as $f_{\mathrm{e}}(n) = 0.5$ Hz. The simulated signal was calculated as:

$$\begin{aligned} y(n) = {} & A_{\mathrm{h}}\cos\left(2\pi f_{\mathrm{h}}(n)\frac{n}{f_{\mathrm{s}}} + \phi_{\mathrm{h}}\right) \\ & + A_{\mathrm{b}}\cos\left(2\pi f_{\mathrm{b}}(n)\frac{n}{f_{\mathrm{s}}} + \phi_{\mathrm{b}}\right) \\ & + A_{\mathrm{e}}\cos\left(2\pi f_{\mathrm{e}}(n)\frac{n}{f_{\mathrm{s}}} + \phi_{\mathrm{e}}\right), \end{aligned} \tag{10}$$

where ϕ_{h}, ϕ_{b}, and ϕ_{e} are random phases with uniform distribution and are associated with the heart rate, respiratory rate, and noise signals, respectively. The amplitude values of A_{h} and A_{b} were set to 10 and 1, respectively. We generated 6,000 samples with a sampling rate of 100 Hz. We set the model order to 30 for the Burg method based on AIC, and thus, for a fair comparison we initially set the model order to 30 also for the OPS. Thus, p_{ini} was set to 30 and τ_{th} was set to 25 (via Eq. 9) for the OPS method. For the noise signal, we set $f_{\mathrm{e}}(n)$ to 0.5 Hz. To systematically investigate the effect of varying noise levels on Burg and OPS methods, we increased the noise amplitude starting from 0.1 to 1 at an increment of 0.1. For each chosen noise amplitude, 100,000 output signals were generated. To determine the accuracy of the two methods in predicting the true frequency of 0.3 Hz, we evaluated the following:

$$\left|\hat{R} - R\right| < 0.01, \tag{11}$$

where $\hat{R}$ is the estimated respiratory rate and R is the true respiratory rate of 0.3 Hz. Thus, we counted how many times among 100,000 trials each method was able to satisfy the condition of Eq. (11). The results are provided in Fig. 3 (left panel), where the asterisks indicate the significant difference ($p < 0.05$) between OPS and Burg methods. Clearly, the OPS provides better accuracy than Burg's method for all noise amplitudes (A_{e}) except for the amplitude values of 0.1, 0.9, and 1.0. For amplitude values of 0.9 and 1.0, the noise contamination is so severe, that both methods have trouble identifying the correct frequency of 0.3 Hz. For the negligibly low amplitude value of 0.1, both methods have no problem identifying the correct frequency of 0.3 Hz. For statistical difference, the t-test ($p < 0.05$) was used, and we observed significant difference between the two algorithms when $A_{\mathrm{e}} = 0.2$, 0.3, 0.4, 0.5, 0.6, and 0.7.

To examine the effect of white noise, we used the following equation:

$$\begin{aligned} y(n) = {} & A_{\mathrm{h}}\cos\left(2\pi f_{\mathrm{h}}(n)\frac{n}{f_{\mathrm{s}}} + \phi_{\mathrm{h}}\right) \\ & + A_{\mathrm{b}}\cos\left(2\pi f_{\mathrm{b}}(n)\frac{n}{f_{\mathrm{s}}} + \phi_{\mathrm{b}}\right) + E_{\mathrm{GWN}}, \end{aligned} \tag{12}$$

where all parameters are set to the same values as in Eq. (3). We investigated several different levels of the signal-to-noise ratios (SNRs): −20 dB, −10 dB, 0 dB, 10 dB, and 20 dB. The simulations were performed 100,000 times for each SNR, and the corresponding accuracy of the two methods in predicting the true frequency of 0.3 Hz was evaluated via Eq. (11) with the threshold value set to 0.001. We used a more stringent threshold value than the colored noise simulation since additive GWN had less noise corruptive effect. We counted how many times among 100,000 trials each method was able to satisfy the condition of Eq. (11).

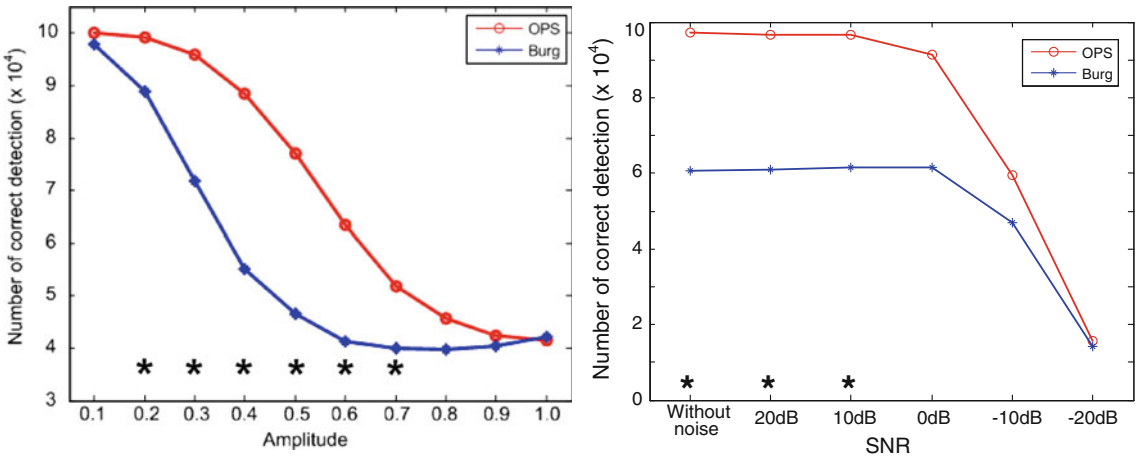

FIGURE 3. The number of correct respiratory rates via 100,000 realizations based on color noise (*left panel*) and white noise (*right panel*); (*left panel*) each amplitude of A_e: $f_b(n)$ and $f_e(n)$ and A_b are set to 0.3 Hz, 0.5 Hz, and 1, and A_e change from 0.1 to 1; (*right panel*) heart rate and respiratory rate are corrupted by additive white Gaussian noise based on several different levels of the signal-to-noise ratios (SNRs): −20 dB, −10 dB, 0 dB, 10 dB, and 20 dB. Asterisks indicate the significant difference between OPS and Burg methods.

The results are provided in the right panel of Fig. 3. As shown in Fig. 3, we observe that the OPS provides significantly ($p < 0.05$) better performance than Burg's method for the SNR up to and including 10 dB. For SNR less than 10 dB, the noise contamination is severe enough that there is no statistical difference in the performance of the two methods.

PPG Data Collection on Human Subjects

For the PPG waveform acquisition, we used an MP506 pulse oximeter (Nellcor Oximax, Boulder, CO) with reusable sensor (Durasensor DS-100A), which incorporates a conditioning circuit and has an analog output of 4.864 kHz. PPG waveforms were collected on 15 healthy subjects with metronome respiratory rates ranging from 0.2 to 0.6 Hz at an increment of 0.1 Hz, and eight healthy subjects with true respiratory rates of 0.7 and 0.8 Hz. We categorized the respiratory rates of 0.2 and 0.3 Hz as low frequency (LF), the rates of 0.4 to 0.6 Hz as high frequency (HF), and the rates of 0.7 and 0.8 Hz as ultra high frequency (UHF). Among the 15 healthy subjects, seven females and eight males age 21.0 ± 1.2 years were involved, and the eight healthy subjects for the UHF experiment were comprised of one female and seven males, age 28.4 ± 3.6 years. None of the subjects had cardiorespiratory or related pathologies. The PPG waveforms were collected in the supine and upright positions, and the sensor was attached to the subjects' left index or middle fingers. The subjects were instructed to breathe at a constant rate according to a timed beeping sound; the subjects inhaled and exhaled when the beeping sound was heard. Three minutes of PPG waveforms were collected for each subject and each position. A true respiration signal was also measured using the Respitrace system, which uses inductive plethysmography to provide calibrated voltage outputs corresponding to rib cage and abdominal compartment volume changes. From the true respiratory signals, true respiratory rates were evaluated by counting the number of peaks.

For both PPG waveforms and respiratory signals, we used the PowerLab/4sp (ADInstruments, Inc., Colorado Springs, CO) for data acquisition. The PowerLab/4sp was connected to a laptop via Universal Serial Bus (USB), and the Chart v4.2.2 software was used to sample the analog signal at 200 Hz. Each 3 min of PPG waveform sampled at 200 Hz were low-pass filtered to 10 Hz. We performed the respiratory rate estimation on 30-s segments of the PPG waveforms, but the segment start was shifted by only 10 s for the entire 3 min recording. Thus, each 30-s segment waveform had a 20-s overlap, and 16 segments were obtained for the entire recording. We set the model order to 30 for both OPS and the Burg method. Our choice of the model order is larger than for the simulation examples because this creates a more challenging scenario for the experimental data.[11] Our proposed AR method was compared to the Burg's algorithm which relies on the AIC to obtain a model order. For quantitative comparison of the two methods, a root mean square error (RMSE) between $\hat{R}_s$ and R_s was computed, where $\hat{R}_s$ and R_s represent an estimated and a true respiratory rate of the sth segment from the PPG waveform, respectively. For every subject, 16 $\hat{R}_s$ and R_s are estimated and counted, respectively (i.e., $s = \{1, 2, \ldots, 16\}$). After calculating RMSEs of all segments, the median

and variance as well as the 5th, 10th, 25th, 75th, 90th, and 95th percentiles were computed across the entire population: 15 subjects of LF and HF, and 8 subjects of UHF.

RESULTS

Figures 4 and 5 show the RMSEs distribution of each method for LF (0.2–0.3 Hz), HF (0.4–0.6 Hz), and UHF (0.7–0.8 Hz) during upright and supine positions, respectively. In Figs. 4 and 5, the circles (red) above and below each method represent the 95th and the 5th percentiles of the all data segments of every subject, respectively. Whiskers (blue) above and below represent the 90th and the 10th percentiles, respectively. The bars above, middle, and below represent the 75th, the 50th, and the 25th percentiles, respectively. Asterisks indicate the significant difference between OPS and Burg methods ($p < 0.05$ with single asterisk and $p < 0.01$ with double asterisks). Tables 2 and 3 summarize the medians and variances of the RMSEs and statistical significance for the upright position (Table 2) and supine position (Table 3), respectively.

For the median and variance of RMSEs in Table 2, OPS was lower than Burg in the upright position for all respiratory rates considered. In the LF range, the median and variance of OPS were 2.10 and 1.96 times smaller than those of Burg, respectively, and these results are statistically significant with $p < 0.01$. In the HF range, the median and variance of OPS were 1.18 and 1.33 times smaller than those of Burg, respectively, and these results are statistically significant with $p < 0.05$. In the UHF range, the median and variance of OPS were 1.08 and 3.84 times smaller than those of Burg, respectively, and these results are statistically significant with $p < 0.05$.

For the median and variance of RMSEs in Table 3, OPS was lower than Burg in the supine position for all respiratory rates considered. In the LF range, the median and variance of OPS were 7.54 and 1.13 times

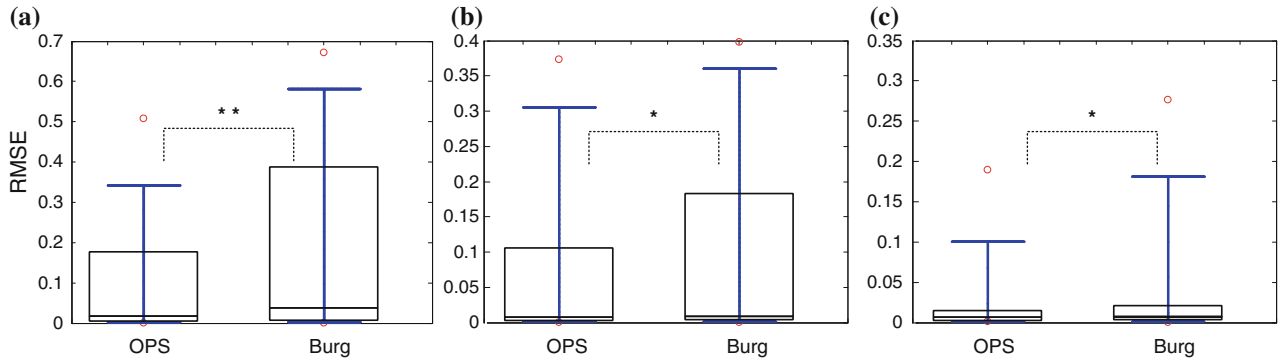

FIGURE 4. RMSEs distribution for the upright position: (a) LF range (0.2–0.3 Hz), (b) HF range (0.4–0.6 Hz), and (c) UHF range (0.7–0.8 Hz). The circles (*red*) above and below each method represent the 95th and the 5th percentiles of the 16 segments for every subject, respectively. Whiskers (*blue*) above and below represent the 90th and the 10th percentiles, respectively. The bars above, middle, and below represent the 75th, the 50th, and the 25th percentiles, respectively. Asterisks indicate the significant difference between OPS and Burg methods ($p < 0.05$ with single asterisk and $p < 0.01$ with double asterisks).

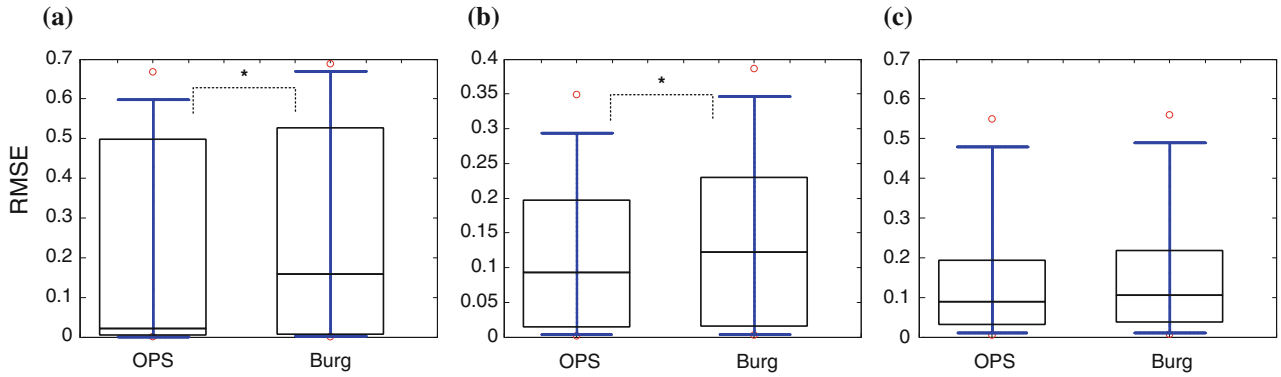

FIGURE 5. RMSEs distribution for the supine position: (a) LF range (0.2–0.3 Hz), (b) HF range (0.4–0.6 Hz), and (c) UHF range (0.7–0.8 Hz). The circles (*red*) above and below each method represent the 95th and the 5th percentiles of the 16 segments for every subject, respectively. Whiskers (*blue*) above and below represent the 90th and the 10th percentiles, respectively. The bars above, middle, and below represent the 75th, the 50th, and the 25th percentiles, respectively. Asterisks indicate the significant difference between OPS and Burg methods ($p < 0.05$ with single asterisk).

TABLE 2. Medians and variances of RMSE for upright position according to respiratory ranges from 0.2 to 0.8 Hz, and corresponding statistical significance.

Position	True breathing rate (Hz)	OPS		Burg		Statistical difference
		Median of RMSE	Variance of RMSE	Median of RMSE	Variance of RMSE	
Upright	LF (0.2–0.3)	0.0177	0.0283	0.0372	0.0554	$p < 0.01$
	HF (0.4–0.6)	0.0077	0.0161	0.0091	0.0214	$p < 0.05$
	UHF (0.7–0.8)	0.0066	0.0037	0.0071	0.0142	$p < 0.05$

TABLE 3. Medians and variances of RMSE for supine position according to respiratory ranges from 0.2 to 0.8 Hz, and corresponding statistical significance.

Position	True breathing rate (Hz)	OPS		Burg		Statistical difference
		Median of RMSE	Variance of RMSE	Median of RMSE	Variance of RMSE	
Supine	LF (0.2–0.3)	0.0211	0.0653	0.1591	0.0735	$p < 0.05$
	HF (0.4–0.6)	0.0926	0.0134	0.1223	0.0168	$p < 0.05$
	UHF (0.7–0.8)	0.0888	0.0299	0.1046	0.0317	

smaller than those of Burg, respectively, with $p < 0.05$. In the HF range, the median and variance of OPS were 1.32 and 1.25 times smaller than those of Burg, respectively, with $p < 0.05$. In the UHF range, the median and variance of OPS were 1.18 and 1.06 times smaller than those of Burg, respectively, but these values were not statistically significant. In summary, the OPS provides significantly higher accuracy than does Burg's method for all respiratory rates for the upright position, while in the supine position it provides higher accuracy in the LF and HF ranges.

CONCLUSION

We presented an AR model using the OPS algorithm to extract respiratory rates directly from pulse oximeter recordings. We compared the OPS's performance against the Burg algorithm, which is one of the widely used approaches in practice. The proposed AR model technique, the OPS, showed significantly higher accuracy than did the Burg method for all respiratory rates for the upright position and in the LF and HF ranges for the supine position. In addition, the OPS was less sensitive to the data segment lengths of the PPG waveforms. To examine the effect of the segment length on our algorithm, we varied data segment length from 15 to 60 s for the PPG waveforms of all subjects, and evaluated the median of RMSEs for all respiratory rates and body positions. These results are shown in Fig. 6. In general, the median of RMSEs were nearly constant from 30 to 60 s segments. Note that artifacts in the PPG waveform have a profoundly deleterious effect when the segment length is <20 s.

We note greater estimation errors with higher breathing rates for the supine position. We believe this

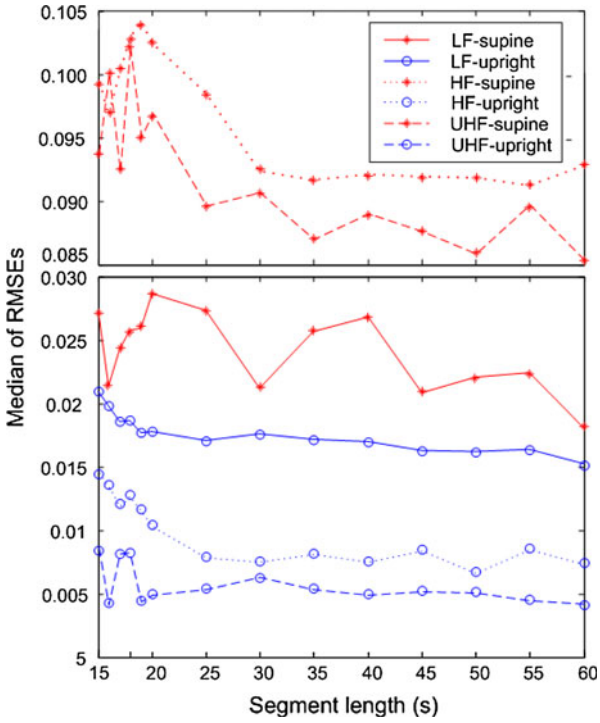

FIGURE 6. Averages of absolute median errors according to time length for estimating respiratory rates.

is because the depth of breathing is less pronounced with higher breathing rates, especially during the supine position. In other words, the amplitude modulation effect of the respiratory sinus arrhythmia on the heart rate becomes less pronounced with higher breathing rates, resulting in greater estimation errors.

While in this study we have limited the extraction of respiratory rates to no greater than 48 breaths/min, our future goal is to extend the capability of the OPS-based AR method so that it can be applicable even

during exercise, which causes higher breathing rates than those examined in this work. Our laboratory is currently exploring using particle filtering methods combined with the OPS for achieving extraction of breathing rates for wide ranges including exercise, all directly from pulse oximeter recordings.

We have previously shown that a nonparametric approach based on the time–frequency spectral method, the variable frequency complex demodulation (VFCDM) approach, provided accurate extraction of respiratory rates in the low frequency range (<0.6 Hz).[5] In addition, it was found that the AR method based on Burg's algorithm was not as robust as the VFCDM approach for these low frequency respiratory rates.[5] The AR method based on OPS, while more accurate than the Burg's algorithm, was not as robust as the VFCDM approach for these low frequency respiratory rates (not shown). However, it is our opinion that AR-based methods combined with particle filters may be more advantageous for greater than 36 breaths/min analysis than time–frequency methods such as the VFCDM or wavelet approaches. Furthermore, we believe that AR-based methods may achieve higher computational speeds than nonparametric methods, thereby being more attractive for real-time implementation of the algorithm. We hope to report about further investigation of these conjectures in a forthcoming publication.

REFERENCES

[1]Ables, J. G. Maximum entropy spectral analysis. *Astron. Astrophys. Suppl.* 15(1):383–393, 1974.

[2]Burg, J. P. Maximum entropy spectral analysis. In: Proc. 37th Annu. Int. SEG Meet. Oklahoma City, 1967.

[3]Chon, K. H., S. Dash, and K. Ju. Estimation of respiratory rate from photoplethysmogram data using time–frequency spectral estimation. *IEEE Trans. Biomed. Eng.* 56(8):2054–2063, 2009.

[4]Faes, L., G. Nollo, and K. H. Chon. Assessment of Granger causality by nonlinear model identification: application to short-term cardiovascular variability. *Ann. Biomed. Eng.* 36(3):381–395, 2008.

[5]Fleming, S. G. A Comparison of signal processing techniques for the extraction of breathing rate from the photoplethysmogram. *Int. J. Biomed. Sci.* 2(1):232–236, 2007.

[6]Lu, S., K. H. Ju, and K. H. Chon. A new algorithm for linear and nonlinear ARMA model parameter estimation using affine geometry. *IEEE Trans. Biomed. Eng.* 48(10):1116–1124, 2001.

[7]Marple, J. S. L. Digital Spectral Analysis with Applications. Englewood Cliffs, NJ: Prentice-Hall, 1987.

[8]Shelley, K. H., A. A. Awad, R. G. Stout, and D. G. Silverman. The use of joint time frequency analysis to quantify the effect of ventilation on the pulse oximeter waveform. *J. Clin. Monit. Comput.* 20(2):81–87, 2006.

[9]Trainin, N., M. Burger, and A. M. Kaye. Some characteristics of a thymic humoral factor determined by assay in vivo of DNA synthesis in lymph nodes of thymectomized mice. *Biochem. Pharmacol.* 16(4):711–720, 1967.

[10]Wang, H., S. Lu, K. Ju, and K. H. Chon. A new approach to closed-loop linear system identification via a vector autoregressive model. *Ann. Biomed. Eng.* 30(9):1204–1214, 2002.

[11]Wang, H., K. Siu, K. Ju, and K. H. Chon. A high resolution approach to estimating time–frequency spectra and their amplitudes. *Ann. Biomed. Eng.* 34(2):326–338, 2006.

[12]Xiao, X., Y. Li, and R. Mukkamala. A model order selection criterion with applications to cardio-respiratory-renal systems. *IEEE Trans. Biomed. Eng.* 52(3):445–453, 2005.

[13]Zou, R., and K. H. Chon. Robust algorithm for estimation of time-varying transfer functions. *IEEE Trans. Biomed. Eng.* 51(2):219–228, 2004.

[14]Zou, R., H. Wang, and K. H. Chon. A robust time-varying identification algorithm using basis functions. *Ann. Biomed. Eng.* 31(7):840–853, 2003.